




Efficient spiral in-out and EPI balanced steady-state free precession cine imaging using a high-performance 0.55T MRI

Matthew C. Restivo  | Rajiv Ramasawmy | W. Patricia Bandettini | Daniel A. Herzka |
Adrienne E. Campbell-Washburn  

Cardiovascular Branch, Division of Intramural Research, National Heart, Lung, and Blood Institute, National Institutes of Health, Bethesda, Maryland

Correspondence

Adrienne E. Campbell-Washburn,
Cardiovascular Branch, Division of
Intramural Research, National Heart, Lung,
and Blood Institute, National Institutes
of Health, 10 Center Dr., Rm B1D47,
Bethesda, MD 20892, USA.
Email: adrienne.campbell@nih.gov

Funding information

This work is funded by the Division of
Intramural Research, National Heart, Lung,
and Blood Institute (Z01-HL006213,
Z01-HL006214).

Purpose: Low-field MRI offers favorable physical properties for SNR-efficient long readout acquisitions such as spiral and EPI. We used a 0.55 tesla (T) MRI system equipped with high-performance hardware to increase the sampling duty cycle and extend the TR of balanced steady-state free precession (bSSFP) cardiac cine acquisitions, which typically are limited by banding artifacts.

Methods: We developed a high-efficiency spiral in-out bSSFP acquisition, with zeroth- and first-gradient moment nulling, and an EPI bSSFP acquisition for cardiac cine imaging using a contemporary MRI system modified to operate at 0.55T. Spiral in-out and EPI bSSFP cine protocols, with TR = 8 ms, were designed to maintain both spatiotemporal resolution and breath-hold length. Simulations, phantom imaging, and healthy volunteer imaging studies ($n = 12$) were performed to assess SNR and image quality using these high sampling duty-cycle bSSFP sequences.

Results: Spiral in-out bSSFP performed favorably at 0.55T and generated good image quality, whereas EPI bSSFP suffered motion and flow artifacts. There was no difference in ejection fraction comparing spiral in-out with standard Cartesian imaging. Moreover, human images demonstrated a $79\% \pm 21\%$ increase in myocardial SNR using spiral in-out bSSFP and $50\% \pm 14\%$ increase in SNR using EPI bSSFP as compared with the reference Cartesian acquisition. Spiral in-out acquisitions at 0.55T recovered $69\% \pm 14\%$ of the myocardial SNR at 1.5T.

Conclusion: Efficient bSSFP spiral in-out provided high-quality cardiac cine imaging and SNR recovery on a high-performance 0.55T MRI system.

KEYWORDS

bSSFP, cardiac cine, EPI, low field, spiral in-out

Matthew C. Restivo and Rajiv Ramasawmy contributed equally to this work.

Published 2020. This article is a U.S. Government work and is in the public domain in the USA.

1 | INTRODUCTION

Clinical MR for cardiac imaging typically uses 1.5 tesla (T) systems and, less commonly, 3T systems, despite the availability of higher field MRI. There are potential advantages to lower field (<1.5T) for cardiovascular applications, which has generated recent interest in low-field cardiac MRI.¹⁻³ Low field may offer reduced costs, reduced artifacts, and improved safety for cardiac imaging.

At lower fields, T_1 is shorter and T_2^* is longer, both favorable for fast gradient echo cardiac imaging sequences. RF power scales quadratically with field strength, which leads to improved safety for cardiovascular implanted electronic devices and metallic devices used for MRI-guided cardiovascular catheterization procedures.^{4,5} The reduced specific absorption rate constraints also permit imaging with higher flip angles.² Increased main magnetic field (B_0) homogeneity at low field provides linear scaling of absolute susceptibility.⁶ Moreover, low-field systems have intrinsically lower cost due to reduced cost of magnet manufacturing and electronics, including amplifiers, as well as potentially reduced siting costs.¹

Balanced steady-state free precession (bSSFP) is the workhorse sequence for cardiac MRI. bSSFP imaging is contingent on fast gradients to achieve gradient moment balancing and on field homogeneity to limit banding artifacts. bSSFP cardiac imaging was not clinically adopted until after 1999 when high-performance gradients were ubiquitous.^{7,8} We recently described a 0.55T MRI system with hardware suitable for technically demanding cardiac imaging, including high-performance gradient specifications (45 mT/m maximum gradient amplitude, 200 T/m/s maximum slew rate).⁹ With the exception of the 0.35T system by View Ray (MRidian, ViewRay, Oakwood Village, OH),^{1,2} commercially available low-field systems have not been paired with both the gradient performance and the field uniformity suitable for bSSFP imaging.

There is an opportunity to increase sampling efficiency of bSSFP imaging at lower field strength and hence to improve SNR-efficiency. At 1.5T, the TR of bSSFP is kept short to limit phase accrual in the presence of B_0 inhomogeneity to avoid off-resonance banding artifacts. At lower field, TR can be lengthened with increased tolerance to banding artifacts, and sampling duration can be prolonged, exploiting the long T_2 and T_2^* . Because SNR scales with the time spent sampling the signal ($\text{SNR} \propto \sqrt{T_{\text{sampling}}}$),¹⁰ prolonged data sampling using spiral or EPI acquisitions can be leveraged to mitigate the SNR loss at low field. Spiral and EPI bSSFP implementations at 1.5T have been limited in their readout length and can suffer from blurring, ghosting, and flow artifacts due to off-resonance.¹¹⁻¹⁴

We modify bSSFP cine acquisitions to exploit our combination of lower field strength and high-performance hardware. For bSSFP cine imaging at 0.55T, we sought to maximize sampling duty cycle while maintaining breath-hold duration,

spatiotemporal resolution, and banding artifacts constant. In this study, we designed efficient spiral in-out and EPI bSSFP cine acquisitions. Simulations, phantom imaging, and in vivo cardiac MR studies were performed to evaluate image quality and SNR with high-efficiency acquisition strategies at 0.55T.

2 | METHODS

2.1 | MRI system

A 1.5T system (Magnetom Aera, Siemens Healthcare, Erlangen, Germany) was modified to operate at 0.55T. The transmit coil, local receiver coils, and system components were retuned for operation at 23.6 MHz. RF amplifiers were replaced for lower frequency transmission. The high-performance shielded gradient system was maintained (maximum gradient amplitude $G_{\text{max}} = 45$ mT/m, maximum slew rate $S_{\text{max}} = 200$ T/m/s), as was the contemporary receiver chain. Local receiver coils were also retuned for operation at 23.6 MHz, and imaging was performed with an 18-channel spine array and a 6-channel body array, with a maximum of 12 spine array channels active during any scan.

2.2 | Simulations

Bloch equation simulations of bSSFP sequences were performed to estimate the maximum achievable SNR at lower field strengths with increased sampling duty cycles. We used field-strength-dependent relaxation parameters from Bottomley et al¹⁵ which defines a model of T_1 across field strengths and assumes a constant T_2 across field strengths. T_1 was calculated using $T_1 = A (\gamma B_0)^B$, with myocardium $A = 0.00158$ and $B = 0.3692$, blood $A = 0.00491$ and $B = 0.3219$, and fat $A = 0.0113$ and $B = 0.1743$. We define sampling duty cycle as ratio of time spent sampling data per TR. Our simulation assumed TR = 3 ms at 1.5T, of which 1 ms is spent acquiring data (33% sampling duty cycle). The TR was varied proportionally with field strength such that the anticipated off-resonance banding tolerance is held constant, resulting in an increased sampling duty cycle at lower field strengths.

Bloch equation simulations were repeated using the sequence parameters of our high sampling duty-cycle spiral in-out and the measured T_1 and T_2 relaxation parameters for 0.55T ($T_{1\text{myo}} = 700$ ms, $T_{1\text{blood}} = 1100$ ms, $T_{1\text{fat}} = 190$ ms, $T_{2\text{myo}} = 60$ ms, $T_{2\text{blood}} = 260$ ms, $T_{2\text{fat}} = 95$ ms)⁹ and compared to simulations of the reference Cartesian acquisition at 1.5T with literature values for T_1 and T_2 ($T_{1\text{myo}} = 950$ ms, $T_{1\text{blood}} = 1500$ ms, $T_{1\text{fat}} = 300$ ms, $T_{2\text{myo}} = 52$ ms, $T_{2\text{blood}} = 250$ ms, $T_{2\text{fat}} = 55$ ms).^{16,17} To assess blurring caused by our spiral in-out acquisition, the point spread function (PSF) was simulated in the presence of off-resonance and myocardial motion.

2.3 | Spiral in-out and EPI bSSFP imaging

Our standard 1.5T cine imaging protocol acquires 30 cardiac frames in a 12 heartbeat breath-hold, with a 312.5 Hz bSSFP passband for TR = 3.2 ms. A 2.7-fold reduction in off-resonance is anticipated at 0.55T, allowing TR = 8.64 ms to preserve tolerance to banding artifacts. We limited TR to 8 ms at 0.55T to minimize sensitivity to motion and flow. Spiral in-out and EPI sequences were designed to maintain identical breath-hold length, spatial resolution, and cine temporal resolution. Sequence parameters are provided in Table 1.

A retraced spiral in-out design was chosen for its efficiency and artifact suppression. Zeroth-order gradient moments (M₀) and first-order gradient moments (M₁) were nulled in all axes to compensate for constant velocity motion.¹⁴ An M₀-balanced spiral in-out waveform is inherently M₁ balanced by symmetry,¹¹ providing robustness to motion and flow as well as a high sampling duty cycle. A retraced spiral in-out trajectory acquires each spiral interleave twice, starting from opposite position in k-space,¹⁸ which is advantageous because the phase accrual due to off-resonance is balanced by the acquisition with the opposite gradient polarity, reducing image blurring and ghosting. Variable-density sampling (VDS) was employed such that the center of k-space is fully sampled and the edges are 60% undersampled (VDS design from: <https://mrsrl.stanford.edu/~brian/vdspiral/>). VDS spiral design enables faster spiral imaging but may result in high-frequency aliasing from undersampling the k-space periphery.^{19,20} Blood-myocardium edge sharpness

was measured in vivo for Cartesian and spiral in-out acquisitions using line profiles. Line profiles were fit using a sigmoid curve,²¹ and the edge sharpness was measured as the pixel distance between 10% and 90% of the signal range.

For EPI bSSFP cine, we used an echo-train length of 5 to achieve matched temporal resolution with the other sequences without acceleration by parallel imaging. TE shifting and M₁ balancing reduce sampling duty cycle and therefore were not used for our EPI protocol. As a result, the EPI bSSFP sequence was susceptible to motion and flow artifacts.

Spiral in-out and EPI image reconstructions were performed using the Gadgetron framework²² (<https://github.com/gadgetron/>) for low-latency inline reconstruction. For spiral image reconstruction, trajectories were corrected inline using a measured gradient system impulse response function.^{23,24} Spiral image reconstruction included 5 conjugate gradient SENSE²⁵ iterations to compensate for the undersampling due to VDS, and density compensation was computed using an iterative method.²⁶ Low-resolution coil sensitivity maps from gridding a filtered portion of the fully sampled center of k-space were used for B₁-weighted coil combination. The spiral in-out bSSFP conjugate gradient SENSE reconstruction required 13s for 30 frames per slice.

2.4 | Phantom imaging

Relative SNR was measured using the T₁ mapping and ECV standardization (TIMES) phantom.²⁷ Vials with T₁ and T₂

TABLE 1 Cine imaging parameters

	Cartesian bSSFP	EPI bSSFP	Spiral in-out bSSFP
Resolution (mm × mm)	1.4 × 1.4	1.4 × 1.4	1.4 × 1.4
FOV (mm × mm)	360 × 270	360 × 308	360 × 360
Slice thickness (mm)	8	8	8
Acceleration factor	2	1	1.25 VDS
Flip angle (degrees)	60	60	60
TRs per frame	108	44	44
TRs per frame per heartbeat	10	4	4
TR (ms)	3.2	8	8
TE (ms)	1.6	4	4
Echoes per TR	1	5	1
Receiver bandwidth (Hz/px)	850	1150	545
Average # of cine frames acquired (heartrate dependent)	31	31	31
Duration (heartbeats)	12	12	12
Sampling duty cycle	0.34	0.52	0.69
Theoretical relative SNR (by $\sqrt{T_{\text{sampling}}}$)	1.00	1.24	1.42

Note: A standard 1.5T Cartesian clinical cine protocol was used, and the EPI and spiral in-out were designed with matched resolution, flip angle, acquired frames, and duration. Theoretical SNR is predicted relative to the Cartesian sequence considering only sampling duty cycle.

bSSFP, balanced steady-state free precession; T_{sampling}, data sampling time; VDS, variable-density sampling.

values representative of myocardium ($T_1 = 820$ ms, $T_2 = 50$ ms) and blood ($T_1 = 1600$ ms, $T_2 = 250$ ms) were selected for comparison. Note that for the most representative vials in this phantom, T_1 values are long compared to in vivo T_1 measured at 0.55T. Pixel-wise SNR was measured using the mean and SD across 100 consecutive measurements of the Cartesian, EPI, and spiral in-out acquisitions.

2.5 | Healthy volunteer imaging

Twelve healthy volunteers (mean age 26.7 ± 8.2 years) underwent cine imaging using the prototype 0.55T MRI system. Volunteers provided written informed consent, and MR imaging was approved by our local institutional review board (clinicaltrials.gov NCT03331380). A short-axis stack (8 to 10 slices) and 3 long-axis slices were acquired with the standard Cartesian and spiral in-out bSSFP cine protocols. Initial in vivo assessment of the imaging protocols confirmed that the EPI bSSFP sequence suffered from flow artifacts as a result of incomplete M1-nulling. Thus, only a single midventricular short-axis slice and a 4-chamber long-axis slice were collected using the EPI bSSFP sequence for the purpose of SNR comparison in static frames. Cine datasets were reconstructed using retrospective triggering and interpolated to 30 temporal frames.²⁸ One heartbeat was used for transition to steady-state, and total breath-hold duration was 10 to 15 s depending on the subjects' heart rate.

In vivo SNR maps were generated using the method of pseudoreplicas.²⁹ Noise prewhitening used a calibration scan to determine the noise covariance matrix and create virtual channels in which the noise in each channel is uncorrelated with a SD of 1.³⁰ Gaussian white noise was added to the prewhitened data (100 pseudo-replicas) to calculate SNR. SNR maps were computed for all volunteers using the same midventricular slice for all 3 sequences. SNR values for myocardium and blood were taken using regions of interest in the septum and left ventricle blood pool at both end-diastole and peak-systole. Blood-myocardium contrast-to-noise ratio (CNR) was calculated as the difference in SNR between the 2 tissues.

Cardiac volumes and function were assessed by manual segmentation performed by an experienced cardiologist. Cardiac volumes were compared using Bland-Altman analysis and coefficients of variation between bSSFP spiral in-out cine and Cartesian cine acquisitions.

Nine subjects returned for a 1.5T exam using a comparable MRI system (Magnetom Aera, Siemens Healthcare) within 5 months. Cartesian cine imaging was performed using the parameters in Table 1. SNR was compared between the optimal spiral in-out bSSFP at 0.55T and clinical Cartesian imaging at 1.5T to assess the SNR recovery achieved with an efficient sampling strategy at 0.55T.

3 | RESULTS

3.1 | Simulations

Figure 1 shows the Bloch equation simulations of bSSFP signal intensity, relative to 1.5T, for blood, myocardial, and fat tissues at a range of field strengths. Magnetic polarization alone reduces the SNR linearly with field strength; however, T_1 shortening at lower field provides some compensation for this signal loss. Moreover, increased TR and sampling duty cycle enable further SNR increase at lower fields. The theoretical signal intensity in the myocardium, blood, and fat at 0.55T are 80%, 70%, and 62% of the signal at 1.5T, respectively, with a hypothetical sampling duty cycle of 87.7%.

The EPI bSSFP sequence used here achieved a sampling duty cycle of 52%, and the spiral in-out bSSFP sequence achieved a sampling duty cycle of 69%, which resulted in a theoretical SNR gain of 24% and 42% over Cartesian bSSFP acquisitions at 0.55T (using $\text{SNR} \propto \sqrt{T_{\text{sampling}}}$). Figure 1C shows the simulated blood and myocardium signal using the measured T_1 and T_2 at 0.55T with the spiral in-out sequence design, compared to Cartesian acquisitions at 0.55T and 1.5T. Theoretically, 0.55T SNR is recovered to 66% and 77% of 1.5T values in the blood and myocardium, respectively, using the proposed spiral in-out sequence. These simulations indicate that bSSFP cardiac image contrast and SNR will be suitable for clinical application at 0.55T using the high sampling duty-cycle sequence.

Relative SNR for the 0.55T Cartesian, EPI, and spiral in-out acquisitions calculated from simulation, phantom measurements, and in vivo measurements are summarized in Table 2.

The PSF FWHM of the spiral in-out acquisition was measured to be 1.14 pixels, indicating a slight blurring (FWHM > 1 pixel) associated with the spiral trajectory. By comparison, the PSF FWHM of the reference Cartesian acquisition was 0.94 pixels. With off-resonance of 80 Hz (equivalent to fat at 0.55T), the PSF FWHM broadened to 1.42 pixels. By comparison at 1.5T, off-resonance of 220 Hz (equivalent to fat) generated a broad PSF FWHM of 2.88 pixels. The center of k-space is acquired 4 times during the 32 ms acquisition window per cardiac frame, leading to additional spatial blurring. Simulated myocardial motion of 4 cm/s³¹ caused the spiral in-out PSF FWHM to broaden to 1.34 pixels. Overall, the blurring caused by the spiral in-out acquisition is < 0.5 pixels in all cases.

3.2 | Phantom imaging

Both the prototype 0.55T MRI system and the 1.5T MRI system had field homogeneity < 0.5 ppm across a 25 cm diameter sphere, indicating that relative field homogeneity

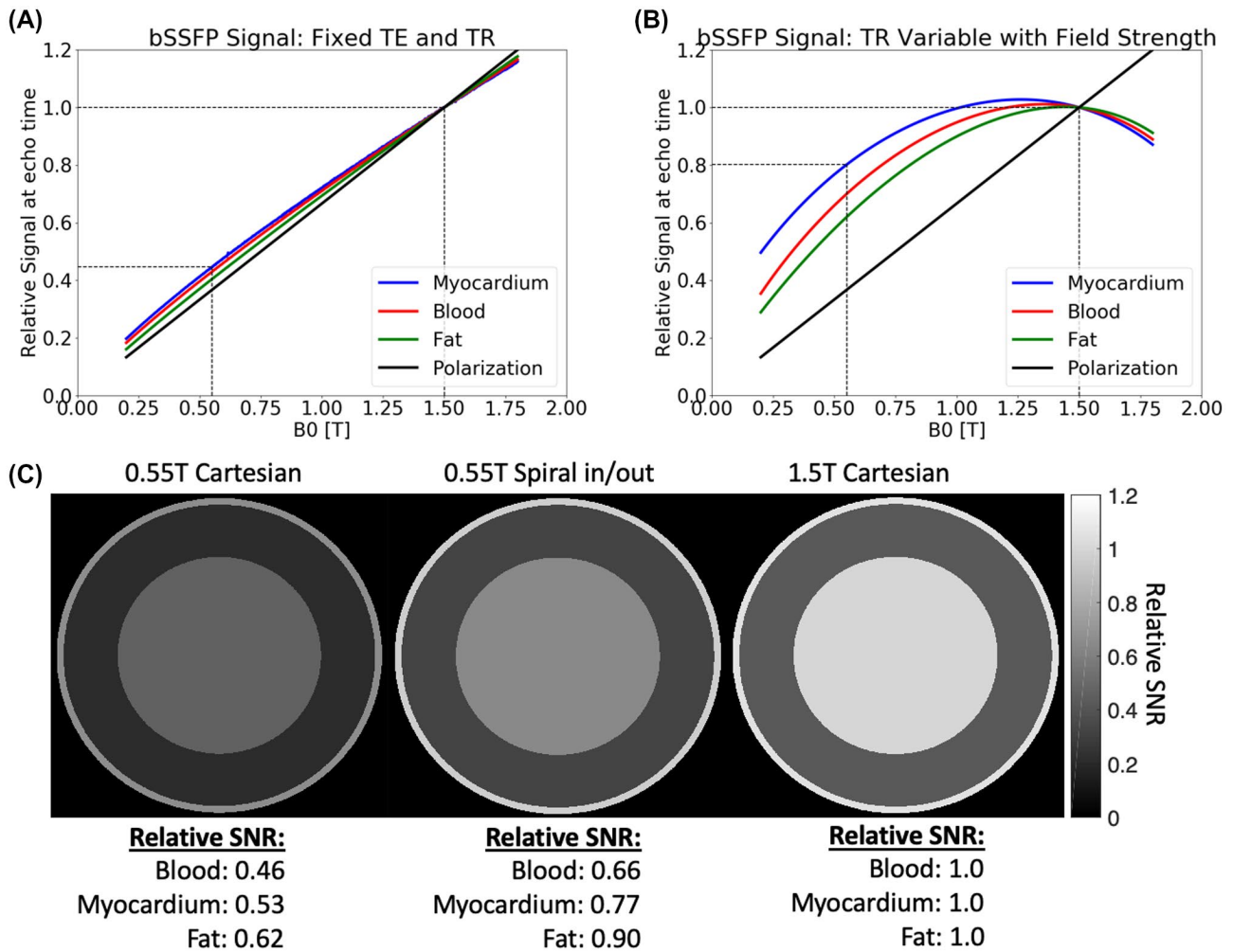


FIGURE 1 Bloch simulation results: bSSFP signal versus field strength. (A) Fixed TE = 1.5 ms and TR = 3 ms for all field strengths results in signal intensity that is nearly proportional to B_0 , with some compensation from T_1 shortening at lower field. (B) Significant increase in simulated signal intensity is achieved when TR and sampling duty cycle vary proportionally to B_0 such that bSSFP banding is kept constant. T_1 and T_2 determined were based on Bottomley et al.¹⁵ (C) Simulated signal intensity comparison using the Cartesian acquisition and proposed spiral in-out acquisition with measured T_1 and T_2 . Signal intensity is scaled relative to blood at 1.5T for display, and relative signal intensity is provided for each tissue type. bSSFP, balanced steady-state free precession; T, tesla

TABLE 2 Relative SNR for blood and myocardium at 0.55T, and relative blood-myocardium CNR

			Cartesian	EPI	Spiral in-out
1	$\sqrt{T_{\text{sampling}}}$	SNR of any tissue	1.00	1.24	1.42
2	Simulation	Myocardium SNR	1.00	1.26	1.45
		Blood SNR	1.00	1.25	1.44
		CNR (blood-myocardium)	1.00	1.24	1.43
3	Phantom measurement	Myocardium SNR	1.00	1.37	1.52
		Blood SNR	1.00	1.31	1.50
		CNR (blood-myocardium)	1.00	1.21	1.45
4	In vivo measurement	Myocardium SNR	1.00	1.50 ± 0.14	1.79 ± 0.21
		Blood SNR	1.00	1.37 ± 0.17	1.69 ± 0.16
		CNR (blood-myocardium)	1.00	1.21 ± 0.32	1.58 ± 0.22

Notes: Values are scaled relative to the Cartesian acquisition at 0.55T. (1) SNR estimated using sampling duty cycle only; (2) SNR estimated using Bloch equation simulation; (3) SNR and CNR measured in phantom for materials with T_1 and T_2 similar to blood and myocardium; and (4) SNR and CNR measured in vivo in 12 healthy volunteers (reported as mean of systole and diastole measurements). CNR, contrast-to-noise ratio.

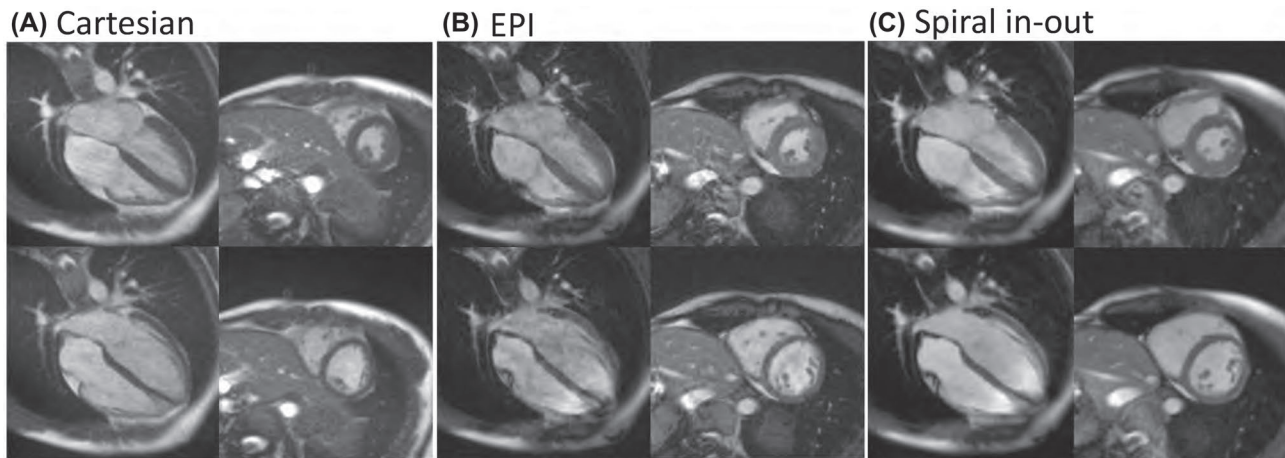


FIGURE 2 (A) Cartesian bSSFP, (B) EPI bSSFP, and (C) spiral in-out bSSFP image quality from a single volunteer. Four-chamber (left) and midventricular short-axis (right) slices are provided at both peak-systole (top) and end-diastole (bottom)

was preserved during system modification. Absolute B_0 field homogeneity in Hz is improved at 0.55T, with < 12 Hz off-resonance at 0.55T and < 32 Hz off-resonance at 1.5T using the spherical phantom. Using the T_1 mapping and ECV standardization phantom, a SNR increase of 37% and 52%, compared to the reference Cartesian sequence, was measured in the vial representing myocardium with EPI and spiral in-out sequences, respectively; and a SNR increase of 31% and 50% was measured in the vial representing blood (Table 2). Phantom CNR was measured to be increased by 21% using EPI and by 45% using spiral in-out, compared to reference Cartesian imaging.

3.3 | Spiral in-out and EPI bSSFP cine imaging

Images from Cartesian, EPI, and spiral in-out bSSFP acquisitions for a midventricular short axis slice and 4-chamber long-axis slice are demonstrated in Figure 2. The EPI bSSFP sequence suffered from motion/flow artifacts due to the unbalanced M1 combined with the long TR (Figure 3). Artifacts can vary with slice position and orientation; thus, multiple slices including a full short-axis stack and 3 long-axis cardiac views are provided in Figure 4, and in Supporting Information Videos S1 and S2 for the Cartesian and spiral in-out acquisitions. Spiral in-out bSSFP provided good image quality, qualitatively, in all slice positions and orientations with high SNR and limited artifacts related to flow and motion. The spiral in-out acquisition permitted clear visualization of trabeculae, coronary arteries, and valves during cine imaging. Edge sharpness measurements showed no increase in blood/myocardium edge blurring between Cartesian and spiral in-out bSSFP (Supporting Information Figure S1).

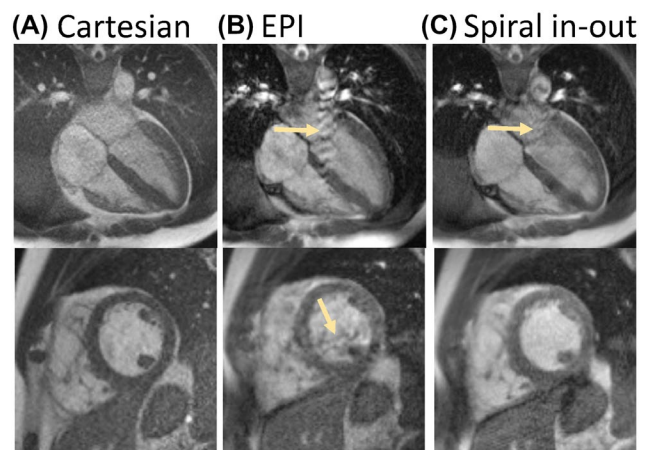


FIGURE 3 Flow artifacts in (A) Cartesian, (B) EPI, and (C) spiral in-out bSSFP sequences (yellow arrows). Flow artifacts are minimal in Cartesian due to short TR. EPI (B) suffers from both ghosting and signal dropout as a result of flow, whereas these artifacts are less disruptive using spiral in-out bSSFP (C)

3.4 | SNR in healthy volunteers

Pixel-wise SNR maps for each sequence showed relative SNR increase with long readout sequences, as expected (Figure 5). Average SNR and CNR values for the 12 healthy volunteers are provided in Table 3. During diastole, the EPI cines yielded a relative SNR increase of $37\% \pm 17\%$ in blood and $50\% \pm 14\%$ in myocardium compared to the reference Cartesian cine. The spiral in-out cines yielded a relative SNR increase of $69\% \pm 16\%$ in blood and $79\% \pm 21\%$ in myocardium during diastole compared to the reference Cartesian cine (Figure 6) (Table 2). CNR was increased by 21% using EPI and 58% using spiral in-out. The deviation from theoretical SNR gains is attributed to the g-factor penalty (< 1.2 , rate 2, GRAPPA reconstruction) for the reference Cartesian

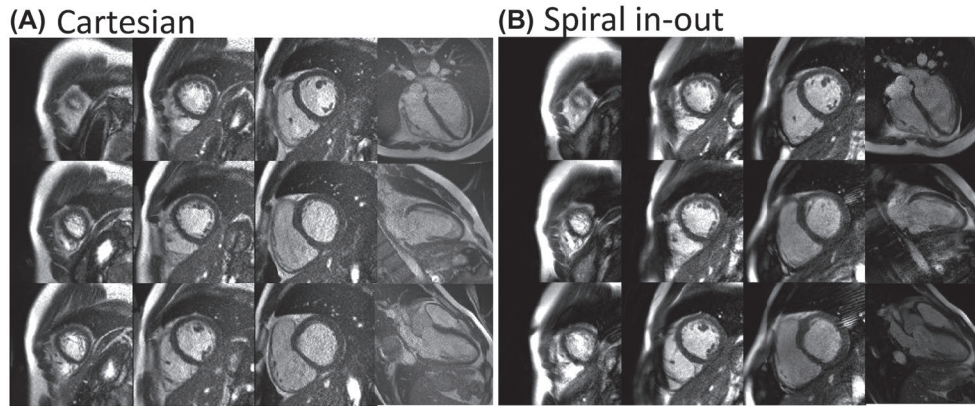


FIGURE 4 Cine images from (A) Cartesian and (B) spiral in-out bSSFP acquisitions. Images from end-diastole are provided for the same volunteer for 9 short axis slices and 4-chamber, 2-chamber, and 3-chamber slices

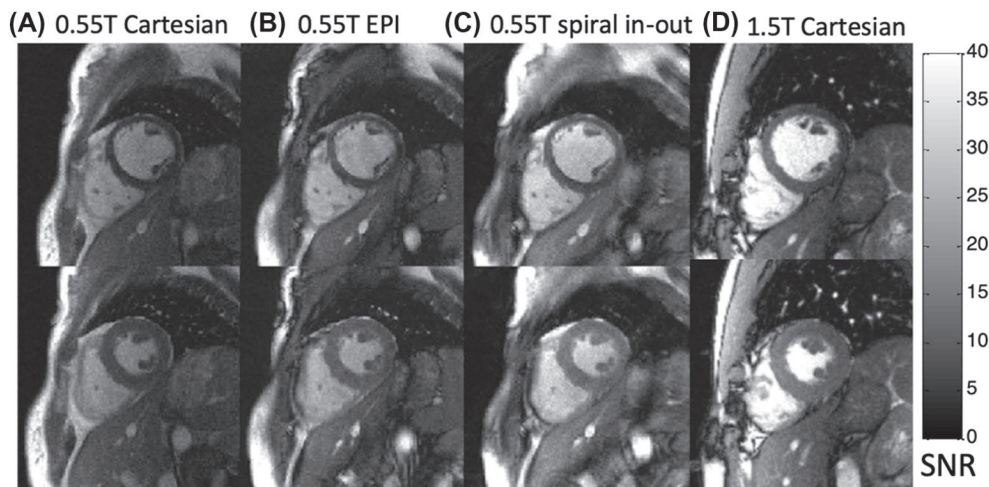


FIGURE 5 Pixel-wise SNR maps for cine frames from 0.55T Cartesian, EPI, and spiral in-out bSSFP acquisitions and 1.5T Cartesian imaging in a single volunteer. Images from end-diastole (top row) and peak systole (bottom row) are provided. Images are displayed in units of SNR.³⁰ T, tesla

TABLE 3 Myocardium and blood SNR of Cartesian, EPI, and spiral in-out bSSFP cine acquisitions using 0.55T

		Cartesian bSSFP	EPI bSSFP	Spiral in-out bSSFP
Myocardium SNR	Diastole	4.9 ± 0.9	7.0 ± 1.5	8.4 ± 2.4
	Systole	5.8 ± 1.0	8.5 ± 2.1	10.6 ± 2.3
Blood SNR	Diastole	13.8 ± 3.0	17.3 ± 4.9	22.7 ± 5.7
	Systole	13.9 ± 3.3	18.5 ± 5.2	22.8 ± 5.2
Blood-myocardium CNR	Diastole	8.9 ± 2.2	10.3 ± 3.6	14.3 ± 3.8
	Systole	8.0 ± 2.3	10.0 ± 3.4	12.2 ± 3.1

Note: SNR is measured at end-diastole and peak systole in a midventricular short axis slice.

acquisition (Figure 7). Assuming a 10% to 20% SNR loss, associated with g-factor, applied only to the reference Cartesian imaging, the relative SNR gains of EPI and spiral in-out acquisitions are as expected.

At 1.5T, systolic SNR was measured to be 16.0 ± 3.3 in the myocardium and 47.0 ± 13.5 in the blood using the

reference Cartesian protocol. This indicates that spiral in-out bSSFP sequence at 0.55T achieved $69\% \pm 14\%$ of the 1.5T SNR in the myocardium and $52\% \pm 15\%$ in the blood, without increasing the total acquisition time. Discrepancies between theoretical SNR and measured in vivo SNR recovery (theoretical SNR recovery: 77% for myocardium and 66%

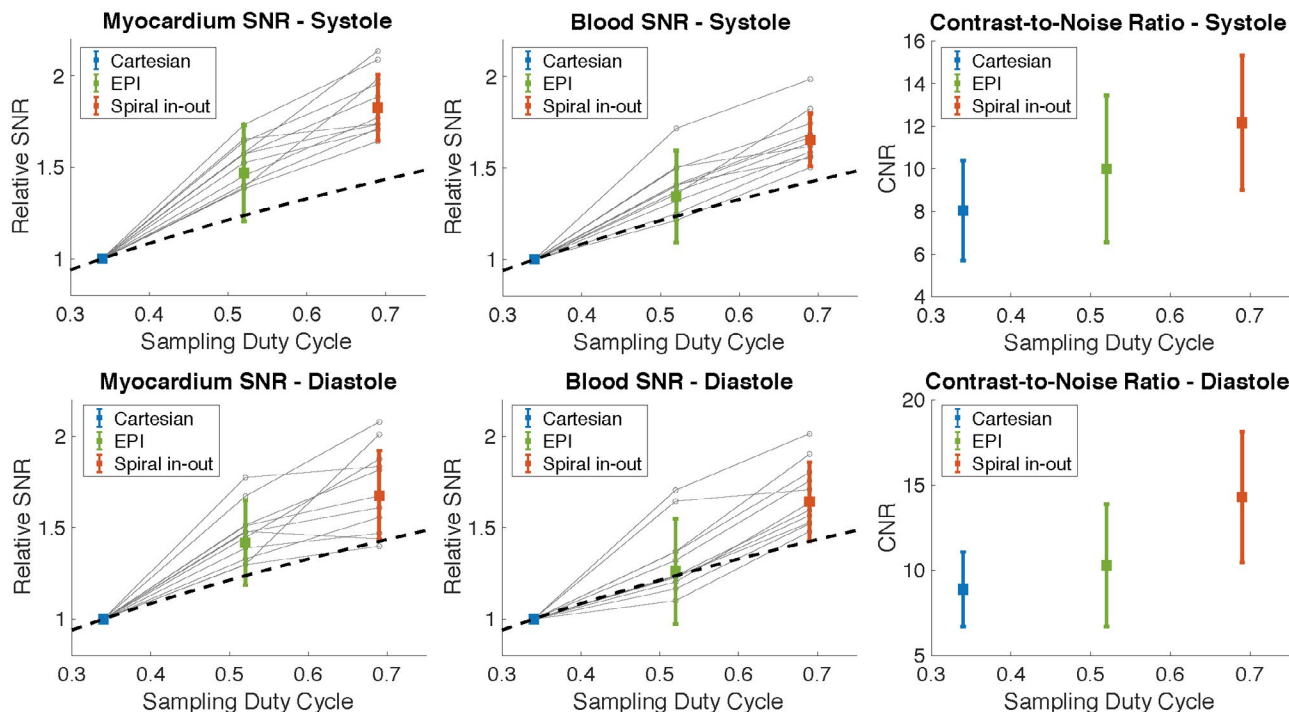


FIGURE 6 Relative myocardial SNR, blood SNR, and blood-myocardium CNR for 12 healthy volunteers at peak-systole and end-diastole (mean \pm SD). Spiral in-out and EPI SNR values are shown relative to reference Cartesian imaging. Gray dots show individual measurements. High variance in SNR for EPI is due to corruption by motion/flow artifact. The dotted line represents theoretical SNR (by $\sqrt{T_{sampling}}$). CNR, contrast-to-noise ratio

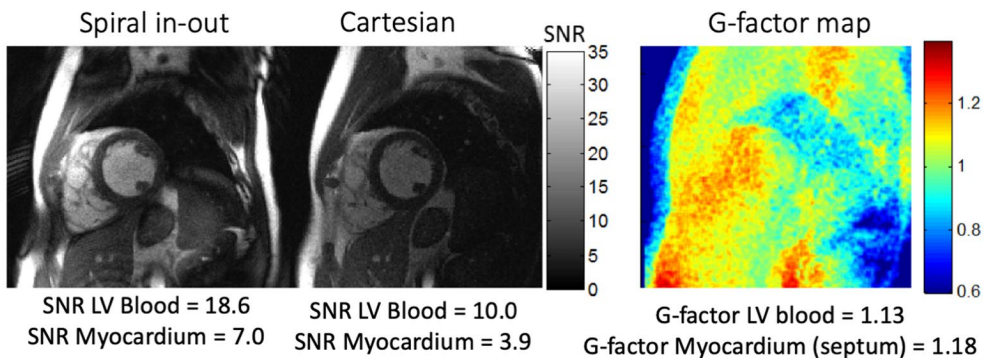


FIGURE 7 SNR maps and g-factor map from a diastolic frame shown for the spiral in-out and Cartesian bSSFP cines in a volunteer with large body habitus. The SNR of the Cartesian cine for LV blood and myocardium are negatively affected by small parallel imaging–induced g-factor (GRAPPA reconstruction, acceleration rate = 2). LV, left ventricular

for blood) are attributed to the suboptimal coil performance on the 0.55T prototype system. By comparing the SNR of a proton density-weighted image (spoiled gradient echo, TE = 3.22 ms, TR = 10000 ms, flip angle = 15 degrees) in a loading phantom at 0.55T and 1.5T using the in vivo coil configurations, we measured a relative SNR of 30%, which is less than the predicted 37% by magnetic polarization for the proton density-weighted image. Therefore, this indicates an SNR penalty of 7% can be attributed to the differences in coil performance between field strengths.

3.5 | Cardiac volumes and function comparison

We compared left ventricular and right ventricular stroke volume and ejection fraction between Cartesian and spiral in-out bSSFP cines from 0.55T. Bland-Altman analysis resulted in a bias of $-0.6\% \pm 2.6\%$ for LVEF, $-1.4\% \pm 4.2\%$ for RVEF, -0.6 ± 6.4 ml for LVSV, and -1.8 ± 6.8 ml for RVSV (Supporting Information Figure S2). Coefficients of variation were calculated to be 2.3% for LVEF, 5.2% for

RVEF, 3.7% for LVSV, and 5.1% for RVSV, which are similar to literature values for the interstudy coefficient of variation (2.4%-4.3%) in healthy volunteers at 1.5T.^{32,33}

4 | DISCUSSION

We used a unique 0.55T system configuration that has high-performance gradients and a superconducting magnet to develop high sampling duty-cycle bSSFP imaging. High sampling duty-cycle sequences are especially attractive at low field to exploit the field homogeneity for longer signal readouts, improved imaging efficiency, limited off-resonance artifacts, and recovery of SNR. We showed that spiral in-out bSSFP generated good quality images using a high-performance prototype 0.55T MRI system. Spiral in-out bSSFP was robust to motion and flow artifacts, in addition to generating 79% increase in myocardial SNR compared to the Cartesian reference and improved blood-myocardium contrast. SNR of the myocardium at 0.55T reached 69% of the SNR at 1.5T using spiral in-out, which is a substantial improvement over the 37% predicted by magnetic polarization alone. Our results illustrate the potential advantages of long readout sequences for image quality and SNR improvement using this high-performance low-field MRI system configuration.

MRI hardware and imaging methods have improved tremendously since the clinical adoption of MRI. Notably, gradient shielding, which eliminates eddy currents that create artifacts during fast imaging sequences, was implemented in 1986³⁴ and therefore was not available in early low-field MRI systems. Simultaneously, 1.5T MRI scanners were commercialized in 1985.³⁵ Fast switching gradients became routine in the early 1990s; previous work has emphasized the importance of gradient performance on achievable SNR and sampling efficiency.³⁶ The SNR-efficiency of spiral imaging is well-documented. Spiral imaging was first demonstrated in 1986³⁷ and was applied for cardiac imaging in 1992³⁸ and functional MRI in 1996.³⁹ These early spiral implementations were spoiled gradient echo acquisitions and used gradient specifications of $G_{\max} = 10$ mT/m and $S_{\max} < 20$ mT/m/ms. bSSFP imaging, which demands fast gradients, was routinely adopted for cardiac imaging after 1999.⁸ Spiral bSSFP followed in 2005¹⁴ and has been more recently optimized for real-time cine imaging.¹¹ To our knowledge, spiral bSSFP has not previously been optimized for either historic or modern lower field MRI systems.

Marques et al³ provide a summary of commercially available low-field scanners, which usually do not have high-performance gradients and typically use permanent magnetic designs. By comparison, the MRI system used here is low field (0.55T) but with high-performance gradients and superconducting magnet design. We are leveraging the modern magnetic design and its associated

field homogeneity, as well as the gradient performance, to achieve prolonged readouts for fast bSSFP imaging. For example, if we implemented our spiral in-out bSSFP sequence using lower performance gradients ($G_{\max} = 22$ mT/m and $S_{\max} = 82$ T/m/s, taken from an average of similar systems³), the TR is extended to 13.7 ms, which is infeasible due to inflow and bSSFP banding artifacts.

We sought to maximize sampling duty cycle for bSSFP cine in this study, and the spiral in-out design provided the highest achievable duty cycle. A spiral-out design could also be used at low field for bSSFP cardiac imaging but requires additional gradients for M1 balancing, which will limit the efficiency compared to spiral in-out.¹⁴ An advantage of spiral-out is motion robustness because the center of k-space is acquired when both M0 and M1 are equal to 0. For spiral in-out bSSFP, M1 is balanced at the end of the TR but not at the TE. At 1.5T, recent implementations of spiral in-out bSSFP cine acquisitions have limited TR to 3.69 ms (with 43% sampling duty cycle) to avoid blurring and banding artifacts.¹¹ Here, we lengthened the TR to 8 ms and increased duty cycle to 69% for our bSSFP acquisitions.

EPI is well established in neuroimaging, where it provides robust fast imaging but is known to be sensitive to flow artifacts. Motion and flow in long-TR EPI bSSFP acquisitions lead to phase discontinuities in k-space; therefore, performance is compromised in the heart, even at low field. Balancing M1 in the phase-encoding direction sacrifices efficiency⁴⁰ and was not explored here. 1.5T implementations of EPI bSSFP cine acquisitions have limited TR to 5.32 ms with 3 echoes per TR to constrain ghosting and flow artifacts. By comparison, our implementation used TR = 8 ms with 5 echoes per TR.

At 1.5T, banding is common between water and fat regions because the resonance of those chemical species falls into separate bSSFP passbands. By design, the long-TR EPI and spiral in-out sequences exhibit banding that is more comparable to 1.5T than the Cartesian reference. At 0.55T, an 8 ms TR creates a stop band with a center frequency within 20 Hz of the dominant fat resonant frequency. This often leads to fluctuating signal intensity within fatty regions as well as total fat signal dropout.

The Cartesian protocol used in this study was identical to our 1.5T clinical protocol and not optimized for low-field imaging. The sampling duty cycle of the Cartesian protocol could be made similar to the spiral by reducing the receiver bandwidth; however, a 2.5 fold increase in undersampling would be required to maintain spatiotemporal resolution, which would introduce an SNR-penalty due to the g-factor of our coil configuration. Current coil geometries (6-channel body coil, 18-channel spine coil) prohibit GRAPPA reconstruction with high undersampling factors. For example, we observed a g-factor of 1.1 to 1.2 in the heart (Figure 7), indicating a 10% to 20% loss in SNR at acceleration rate 2.

We opted to maintain the 1.5T clinical protocol to compare sequences with identical spatiotemporal resolution.

Many factors can influence the measured SNR; our study compares only the SNR of our specific sequences, reconstructions, and imaging procedures. For example, reconstruction implementations, coil geometry, and flip angle choice could alter the measured SNR of our acquisitions and were not explored in detail here in order to directly compare SNR gain due to increased sampling duty cycle. Five iterations were used in the spiral in-out conjugate gradient SENSE reconstruction compared to the GRAPPA or 2D-FFT reconstructions used for Cartesian and EPI. Although iterations can increase image noise,⁴¹ we here only used a modest number of iterations. The method of pseudo-replicas was used to determine the SNR for all acquisitions and is applicable to all reconstruction methods.²⁹ SNR was measured at both systole and diastole because there is a known difference in myocardial signal between cardiac phases.⁴² The increase in CNR for spiral in-out observed in this study can be attributed to decreased noise and not a change in relative contrast because the relative SNR increase in myocardium and blood was approximately the same.

In the future, model-based and compressed sensing reconstructions may allow for higher acceleration factors, improved SNR, and improved image quality for all sequence types. The impact of flip angle on SNR and CNR will also be explored for these high sampling duty cycle sequences. Alternatively, a free-breathing cine⁴³ approach could be implemented to remove the breath-hold constraint on spatiotemporal resolution and improve applicability to patients with disease. The bSSFP spiral in-out acquisition could also be extended to other cardiac sequences, including late-gadolinium enhancement, perfusion, and parametric mapping.^{44,45} Optimization of coils for 0.55T will be explored to improve image quality further, and extension to 3D imaging may alleviate the SNR-penalty associated with poor g-factor.

5 | CONCLUSION

We have demonstrated high sampling duty-cycle bSSFP sequences to generate cardiac cine images using a 0.55T MRI system. Reduced off-resonance allows for increased TR and increased sampling duty cycle, which resulted in high-quality spiral in-out bSSFP cine imaging. This approach exploits the unique properties of our high-performance low-field MRI system.

ACKNOWLEDGMENT

The authors thank the contributions of Christine Mancini and Delaney McGuirt to image acquisition, and the contributions of Margaret (Peg) Lowery and Jennifer Henry to subject recruitment. The authors also thank researchers from Siemens

Healthcare for their assistance in the modification of the MRI system.

CONFLICT OF INTEREST


NHLBI and Siemens Healthcare have a collaborative research and development agreement for diagnostic and interventional MRI, which includes the development of the 0.55T MRI system. Siemens assisted with the modification of the MRI system to operate at 0.55T.

ORCID

Matthew C. Restivo  <https://orcid.org/0000-0002-8655-4594>

Adrienne E. Campbell-Washburn  <https://orcid.org/0000-0002-7169-5693>

TWITTER

Adrienne E. Campbell-Washburn  @ACampbell_MRI

REFERENCES

1. Simonetti OP, Ahmad R. Low-field cardiac magnetic resonance imaging: A compelling case for cardiac magnetic resonance's future. *Circ Cardiovasc Imaging*. 2017;10:e005446.
2. Rashid S, Han F, Gao Y, et al. Cardiac balanced steady-state free precession MRI at 0.35 T: A comparison study with 1.5 T. *Quant Imag Med Surg*. 2018;8:627–636.
3. Marques JP, Simonis FFJ, Webb AG. Low-field MRI: An MR physics perspective. *J Magn Reson Imaging*. 2019;49:1528–1542.
4. Meyer C, Thomas D, Schild H, et al. Low-field magnetic resonance imaging: Increased safety for pacemaker patients? *EP Europace*. 2010;12:952–960.
5. Hoult DI, Phil D. Sensitivity and power deposition in a high-field imaging experiment. *J Magn Reson Imaging*. 2000;12:46–67.
6. Bernstein MA, Huston J III, Ward HA. Imaging artifacts at 3.0T. *J Magn Reson Imaging*. 2006;24:735–746.
7. Scheffler K, Lehnhardt S. Principles and applications of balanced SSFP techniques. *Eur Radiol*. 2003;13:2409–2418.
8. Bundy J, Simonetti O, Laub G, Finn JP. Segmented trueFISP cine imaging of the heart. In Proceedings of the 7th Annual Meeting of ISMRM, Philadelphia, PA, 1999. p. 1282.
9. Campbell-Washburn AE, Ramasawmy R, Restivo MC, et al. Opportunities in interventional and diagnostic imaging by using high-performance low-field-strength MRI. *Radiology*. 2019;293:384–393.
10. Macovski A. Noise in MRI. *Magn Reson Med*. 1996;36:494–497.
11. Feng X, Salerno M, Kramer CM, Meyer CH. Non-Cartesian balanced steady-state free precession pulse sequences for real-time cardiac MRI. *Magn Reson Med*. 2016;75:1546–1555.
12. Herzka DA, Kellman P, Aletas AH, Guttman MA, McVeigh ER. Multishot EPI-SSFP in the heart. *Magn Reson Med*. 2002;47:655–664.
13. Slavin GS, Saranathan M. FIESTA-ET: High-resolution cardiac imaging using echo-planar steady-state free precession. *Magn Reson Med*. 2002;48:934–941.
14. Nayak KS, Hargreaves BA, Hu BS, Nishimura DG, Pauly JM, Meyer CH. Spiral balanced steady-state free precession cardiac imaging. *Magn Reson Med*. 2005;53:1468–1473.

15. Bottomley PA, Foster TH, Argersinger RE, Pfeifer LM. A review of normal tissue hydrogen NMR relaxation times and relaxation mechanisms from 1–100 MHz: Dependence on tissue type, NMR frequency, temperature, species, excision, and age. *Med Phys*. 1984;11:425–448.
16. Baessler B, Schaarschmidt F, Stehning C, Schnackenburg B, Maintz D, Bunck AC. A systematic evaluation of three different cardiac T2-mapping sequences at 1.5 and 3T in healthy volunteers. *Eur J Radiol*. 2015;84:2161–2170.
17. Dabir D, Child N, Kalra A, et al. Reference values for healthy human myocardium using a T1 mapping methodology: Results from the International T1 Multicenter cardiovascular magnetic resonance study. *J Cardiovasc Magn Reson*. 2014;16:69.
18. Fielden SW, Meyer CH. A simple acquisition strategy to avoid off-resonance blurring in spiral imaging with redundant spiral-in/out k-space trajectories. *Magn Reson Med*. 2015;73:704–710.
19. Tsai C-M, Nishimura DG. Reduced aliasing artifacts using variable-density k-space sampling trajectories. *Magn Reson Med*. 2000;43:452–458.
20. Salerno M, Sica C, Kramer CM, Meyer CH. Improved first-pass spiral myocardial perfusion imaging with variable density trajectories. *Magn Reson Med*. 2013;70:1369–1379.
21. Ahmad R, Ding Y, Simonetti OP. Edge sharpness assessment by parametric modeling: application to magnetic resonance imaging. *Concepts Magn Reson Part A Bridg Educ Res*. 2015;44:138–149.
22. Hansen MS, Sørensen TS. Gadgetron: An open source framework for medical image reconstruction. *Magn Reson Med*. 2013;69:1768–1776.
23. Vannesjo SJ, Haeberlin M, Kasper L, et al. Gradient system characterization by impulse response measurements with a dynamic field camera. *Magn Reson Med*. 2013;69:583–593.
24. Campbell-Washburn AE, Xue H, Lederman RJ, Faranesh AZ, Hansen MS. Real-time distortion correction of spiral and echo planar images using the gradient system impulse response function. *Magn Reson Med*. 2016;75:2278–2285.
25. Pruessmann KP, Weiger M, Börner P, Boesiger P. Advances in sensitivity encoding with arbitrary k-space trajectories. *Magn Reson Med*. 2001;46:638–651.
26. Pipe JG, Menon P. Sampling density compensation in MRI: Rationale and an iterative numerical solution. *Magn Reson Med*. 1999;41:179–186.
27. Captur G, Gatehouse P, Keenan KE, et al. A medical device-grade T1 and ECV phantom for global T1 mapping quality assurance—the T1 Mapping and ECV Standardization in cardiovascular magnetic resonance (TIMES) program. *J Cardiovasc Magn Reson*. 2016;18:58.
28. Feinstein JA, Epstein FH, Arai AE, et al. Using cardiac phase to order reconstruction (CAPTOR): A method to improve diastolic images. *J Magn Reson Imaging*. 1997;7:794–798.
29. Robson PM, Grant AK, Madhuranthakam AJ, Lattanzi R, Sodickson DK, McKenzie CA. Comprehensive quantification of signal-to-noise ratio and g-factor for image-based and k-space-based parallel imaging reconstructions. *Magn Reson Med*. 2008;60:895–907.
30. Kellman P, McVeigh ER. Image reconstruction in SNR units: A general method for SNR measurement†. *Magn Reson Med*. 2005;54:1439–1447.
31. Quinones MA, Gaasch WH, Alexander JK. Echocardiographic assessment of left ventricular function with special reference to normalized velocities. *Circulation*. 1974;50:42–51.
32. Grothues F, Smith GC, Moon JC, et al. Comparison of interstudy reproducibility of cardiovascular magnetic resonance with two-dimensional echocardiography in normal subjects and in patients with heart failure or left ventricular hypertrophy. *Am J Cardiol*. 2002;90:29–34.
33. Grothues F, Moon JC, Bellenger NG, Smith GS, Klein HU, Pennell DJ. Interstudy reproducibility of right ventricular volumes, function, and mass with cardiovascular magnetic resonance. *Am Heart J*. 2004;147:218–223.
34. Blamire AM. The technology of MRI—the next 10 years? *Br J Radiol*. 2008;81:601–617.
35. Edelman RR. The history of MR imaging as seen through the pages of radiology. *Radiology*. 2014;273(suppl):S181–200.
36. Reeder SB, McVeigh ER. The effect of high performance gradients on fast gradient echo imaging. *Magn Reson Med*. 1994;32:612–621.
37. Ahn CB, Kim JH, Cho ZH. High-speed spiral-scan echo planar NMR imaging-I. *IEEE Trans Med Imaging*. 1986;5:2–7.
38. Meyer CH, Hu BS, Nishimura DG, Macovski A. Fast spiral coronary artery imaging. *Magn Reson Med*. 1992;28:202–213.
39. Noll DC, Cohen JD, Meyer CH, Schneider W. Spiral K-space MR imaging of cortical activation. *J Magn Reson Imaging*. 1995;5:49–56.
40. Epstein FH, Arai AE. Optimization of fast cardiac imaging using an echo-train readout. *J Magn Reson Imaging*. 2000;11:75–80.
41. Qu P, Zhong K, Zhang B, Wang J, Shen GX. Convergence behavior of iterative SENSE reconstruction with non-Cartesian trajectories. *Magn Reson Med*. 2005;54:1040–1045.
42. Goldfarb JW, McLaughlin J, Gray CA, Han J. Cyclic CINE-balanced steady-state free precession image intensity variations: Implications for the detection of myocardial edema. *J Magn Reson Imaging*. 2011;33:573–581.
43. Xue H, Kellman P, LaRocca G, Arai AE, Hansen MS. High spatial and temporal resolution retrospective cine cardiovascular magnetic resonance from shortened free breathing real-time acquisitions. *J Cardiovasc Magn Reson*. 2013;15:102.
44. Yang Y, Meyer CH, Epstein FH, Kramer CM, Salerno M. Whole-heart spiral simultaneous multi-slice first-pass myocardial perfusion imaging. *Magn Reson Med*. 2019;81:852–862.
45. Shin T, Lustig M, Nishimura DG, Hu BS. Rapid single-breath-hold 3D late gadolinium enhancement cardiac MRI using a stack-of-spirals acquisition. *J Magn Reson Imaging*. 2014;40:1496–1502.

SUPPORTING INFORMATION

Additional Supporting Information may be found online in the Supporting Information section.

FIGURE S1 Edge sharpness comparison between Cartesian and spiral in-out acquisitions. A, Example profiles drawn in the septal wall for both Cartesian and spiral in-out bSSFP images. B, Example intensity profile from a spiral in-out cine frame. Sharpness was measured as the pixel distance between 10 and 90% off the min-max range of a sigmoid fit of the profile. C, Box-plot of sharpness for 12 healthy volunteers,

averaged over all frames. No significant difference was measured between the two sequences

FIGURE S2 Bland-Altman plots comparing Cartesian and spiral in-out cines for left-ventricle and right-ventricle ejection fraction and stroke volume assessment. Mean difference (solid line) and 1.96 standard deviations (dotted lines) are displayed

VIDEO S1 Short axis cine stack acquired using the Cartesian (left) and spiral in-out (right) bSSFP protocols. Increased SNR can be observed using spiral in-out with limited artifacts

VIDEO S2 Three long-axis cine views acquired using the

Cartesian (top row) and spiral in-out (bottom row) bSSFP protocols

How to cite this article: Restivo MC, Ramasawmy R, Bandettini WP, Herzka DA, Campbell-Washburn AE. Efficient spiral in-out and EPI balanced steady-state free precession cine imaging using a high-performance 0.55T MRI. *Magn Reson Med.* 2020;84:2364–2375. <https://doi.org/10.1002/mrm.28278>